

MINIATURIZED METAL MOUNT MINKOWSKI FRACTAL RFID TAG ANTENNA WITH COMPLEMENTARY SPLIT RING RESONATOR

Ali S. A. Jalal^{1, 2, *}, Alyani Ismail^{1, 3}, Adam R. H. Alhawari¹, Mohd F. A. Rasid¹, Nor K. Noordin¹, and Mohd A. Mahdi¹

¹Wireless and Photonic Networks Research Center (WiPNET), Department of Computer and Communication Systems Engineering, Faculty of Engineering, Universiti Putra Malaysia (UPM), Serdang, Selangor 43400, Malaysia

²College of Information Engineering, Al-Nahrain University, Al-Jadriya Complex, Baghdad 10070, Iraq

³Institute of Advanced Technology, Universiti Putra Malaysia, Malaysia

Abstract—This paper proposes miniature radio frequency identification (RFID) tag antenna designed to operate on metallic objects, in the UHF frequency range (915 MHz), without significantly degrading its read range. The antenna structure is composed of two parts: Part 1 comprises two square patches electrically connected to the ground plane through vias while Part 2 is an unconnected inter-layer consisting of two square complementary split ring resonators to allow for capacitive reactance increase. Consequently, its self-resonant frequency will shift towards low frequency, which theoretically allows shrinking RFID tag antenna into smaller size. The antenna was simulated and measured to verify its conjugate matching with chip impedance. The results of experimental tests show that the proposed RFID tag offers a maximum read range of 0.82 m when placed on a metallic object. The tag's overall size is $36.7 \times 18.1 \times 3.165$ mm³. Both simulation and measurement results are provided to validate the design.

1. INTRODUCTION

Radio Frequency Identification (RFID) is a rapidly advancing technology to easily identify objects. Hence, we have found abundant

Received 13 January 2013, Accepted 1 April 2013, Scheduled 8 April 2013

* Corresponding author: Ali Sadeq Abdulhadi Jalal (asaj@ieee.org).

ongoing studies conducted on RFID tag design. For instance, the compact slotted planar inverted (PIFA), orthogonally proximity-coupled patch antenna, double PIFA, PIFA arrays, and patch antenna structures are commonly used in RFID metal tag designs [1–6]. Several fractal antennas were also developed for RFID applications, the compact dual-band printed dipole antenna, rectangular fractal shape radiator element and metal meander patch antenna, compact fractal dipole antenna for 915 MHz and 2.4 GHz, modified Koch fractal dipole antenna [7–12]. The main problem that these designs face is to have high inductive reactance without enlarging the size.

Primarily, RFID tag performance relies heavily upon two factors, antenna gain and impedance matching accuracy [13]. The key factor in determining the performance of metal tags critically relies on accomplishing accurate impedance matching due to the bandwidth insufficiency and low gain characteristics [14]. Therefore, it is important to discover the optimal antenna dimensions to get the required impedance measurement accuracy for the design. There are substantial reports on impedance measurement verification for RFID tag antenna design as our reference in [13, 15–18].

This paper proposes an improvement to the identified weakness of previous enlarged sizes in RFID tag antenna design. It suggests an alternative to miniaturize the antenna size. It is achievable by inserting a floating slotted conductive layer between the top and bottom layers in order to increase the capacitance of the antenna. This layer consists of two basic structures of Split Ring Resonators (SRR) in a square Complementary (CSRR) form. Then, the antenna resonance is shifted to low frequency band to facilitate higher inductance at smaller sized tag antenna. Section 2 presents the proposed antenna design structure integrated with CSRR. Meanwhile Section 3 elaborates the simulation and measurement results. Conclusions are finally discussed in Section 4.

2. ANTENNA DESIGN

This section presents a miniature RFID tag antenna design with two Minkowski fractal structure patches deposited as an upper layer and a ground plane at the bottom layer for metallic objects identification. The structure is inserted with an unconnected inter-CSRR layer. Figure 1 shows the layout of the tag antenna design.

The top layer consists of two symmetrical square fractal patches of the Minkowski type (Figure 1(a)) with a gap m of 0.5 mm separating them. The slot width (W_1) and indentation (W_2) of both patches are

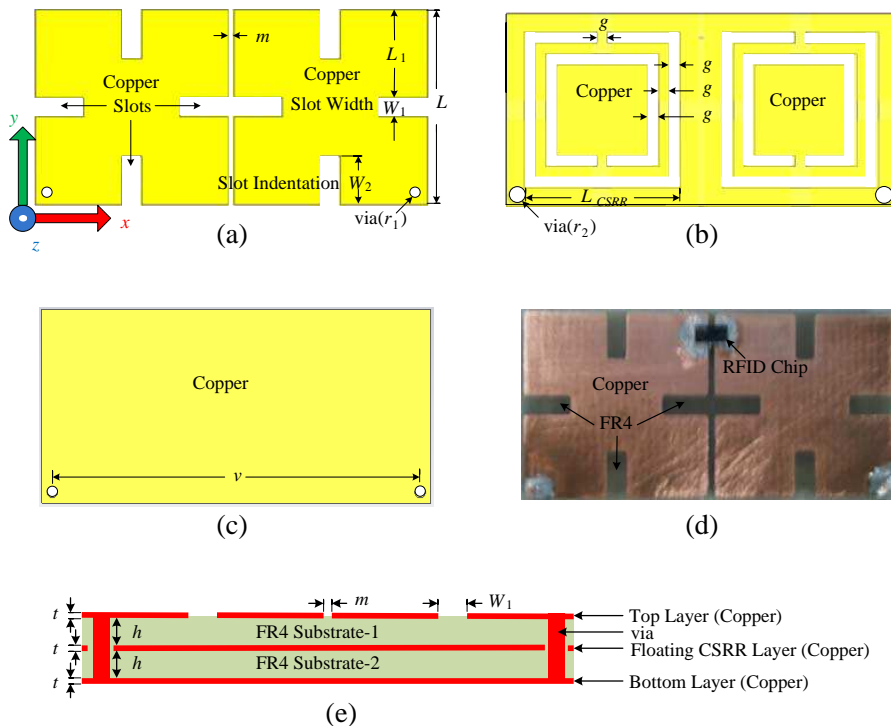


Figure 1. Design arrangement of the proposed fractal RFID tag antenna: (a) upper layer, (b) inter-CSRR layer, (c) bottom layer, (d) photograph of the assembled RFID tag, and (e) side view.

given by

$$W_1 = a_1 L \tag{1}$$

$$W_2 = a_2 L \tag{2}$$

where a_1 and a_2 are the slot width factor and indentation factor, chosen as $a_1 = 0.1$ and $a_2 = 0.25$, respectively, for optimal tag design. The fractal patches and bottom layer are electrically connected to each other by two vias (r_1) as shown in Figures 1(a) and (e); the inter-CSRR layer is floating. Figure 1(b) displays the floating inter-layer containing two CSRRs, each centered underneath one of the two patches with via radius $r_2 > r_1$. Figure 1(d) shows the assembled RFID tag where the chip is attached across the gap between the two fractal patches, opposite to the vias, and connects to both of them. The three copper layers shown in Figures 1(a), (b), and (c) are with thickness $t = 0.035$ mm. They are separated by two FR4 substrates

each of thickness $h = 1.53$ mm, dielectric constant $\epsilon_r = 4.4$, and loss tangent of 0.02 as shown in Figure 1(e). Proposed RFID tag antenna dimensions labeled on Figure 1 are given in Table 1.

Table 1. Antenna dimensions.

Parameter	L	L_1	W_1	W_2	m	r_1	r_2	L_{CSRR}	v	g	h	t
Dimension in mm	18.1	8.145	1.81	4.525	0.5	0.5	0.75	14.6	34.7	1	1.53	0.035

An extensive analysis of the electromagnetic properties of SRRs and CSRRs is already presented in [19–24]. Falcone et al. [25] have shown that if the effects of the metal thickness and losses, as well as those of the dielectric substrate, are neglected, the complementary negative structures of the SRR have dual properties. Thus, when exciting the SRR by an axial magnetic field, it might be considered as a resonant magnetic dipole [19, 22]. Similarly, the CSRR essentially behaves as an electric dipole (with the same resonance frequency of its dual SRR) that can be excited by an axial electric field. The basic structure of the CSRR, as well as the lumped-circuit model proposed in [19, 25] is shown in Figure 2. The resonance frequency of the CSRR is given by $f_o = 1/2\pi\sqrt{L_c C_c}$, where C_c stands for the capacitance of a disk of radius $r_o - c/2$ surrounded by a ground plane at a distance c of its edge, and L_c — is the parallel combination of the two inductances connecting the inner disk to the ground.

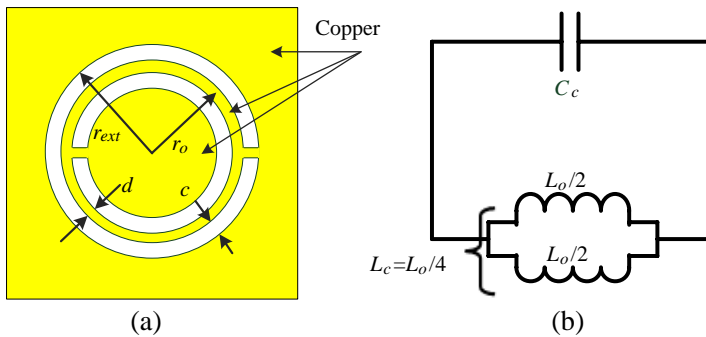


Figure 2. (a) Basic layout of the CSRR. (b) Its lumped circuit model.

Figures 3(a) and (b) depict the lumped-element circuit diagrams of the proposed RFID tag antenna with and without the inter-CSRR layer. Figure 3(b) illustrates that the capacitance considered in the model is doubled while the inductance is halved since two CSRRs are

used in the inter-layer. Figure 3(c) illustrates the complete circuit model of the tag antenna. Accordingly, its resonant frequency can be determined by $f_c = 1/2\pi\sqrt{L_t C_t}$. The inductor L_a is basically from the loop formed by patches, vias, and ground; which can be adjusted by changing the patch length L . The inter-CSRRLayer increases the capacitance by $2C_c$ to the antenna, thereby increasing the total capacitance $C_t = (C_a + 2C_c)$ significantly rather than the added inductance $L_c/2$. Therefore, antenna resonance, f_c shifts down to the low-frequency band. Figure 4 shows the simulated responses of the input impedances of the proposed RFID tag antenna with different fractal patch lengths (L). The figure clearly shows that the larger length of patch (L) results in lower resonant frequency of the RFID tag antenna.

A MURATA RFID magicstrap LXMS31ACNA-010 chip [26], with input impedance of $(12 - j107)\Omega$ at 915 MHz was used for this tag design. The minimum threshold power of the RFID magicstrap is

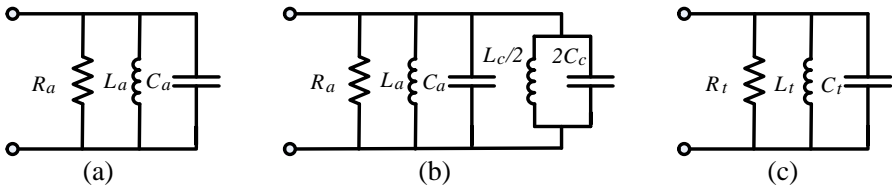


Figure 3. Lumped-element circuit model of (a) proposed tag antenna, (b) proposed tag antenna with an inter-CSRRLayer, and (c) the proposed RFID tag antenna overall equivalent lumped element model.

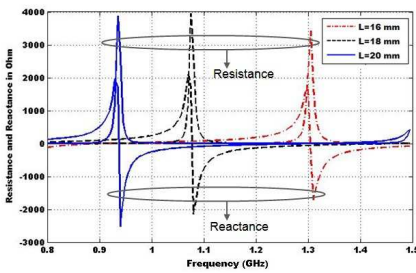


Figure 4. Simulation results of antenna input impedances with different values of fractal patch length L (L as denoted in Figure 1).

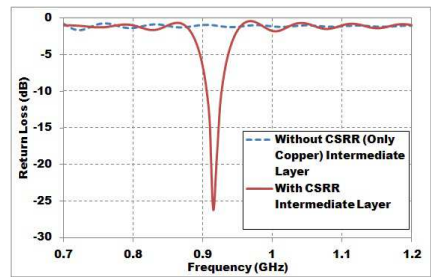


Figure 5. Simulated return loss of the antenna.

-8 dBm ($160 \mu\text{W}$). The antenna's physical dimensions are adjusted until its inductance provides conjugate impedance matching to the RFID used chip, where the resonant frequency of the antenna is accordingly determined. The overall size of the proposed tag antenna is $36.7 \times 18.1 \times 3.165 \text{ mm}^3$.

3. RESULTS AND DISCUSSION

The designed RFID tag antenna was modeled and simulated using full-wave electromagnetic simulator (CST Microwave Studio, 2010) [27]. Tuning of the proposed RFID tag performance was simulated by considering a square metal sheet of 0.5λ side length and 0.006λ thickness as a background spaced 1.0-mm beneath to account for RFID tag casing. Figure 5 shows the return loss of the antenna simulated by considering used chip impedance lumped-element values in CST Microwave Studio. Good resonance is obtained at the operating frequency of 915 MHz when the intermediate layer is composed of two CSRR structures, one under each fractal patch. Figure 5 also demonstrates that the antenna does not resonate if the intermediate CSRR layer is replaced by a full copper one without CSRR slits, which verified the concept of frequency shift due to this layer.

A differential probe reported in [15–18], which had a symmetrical structure, was employed as part of our measurement method to

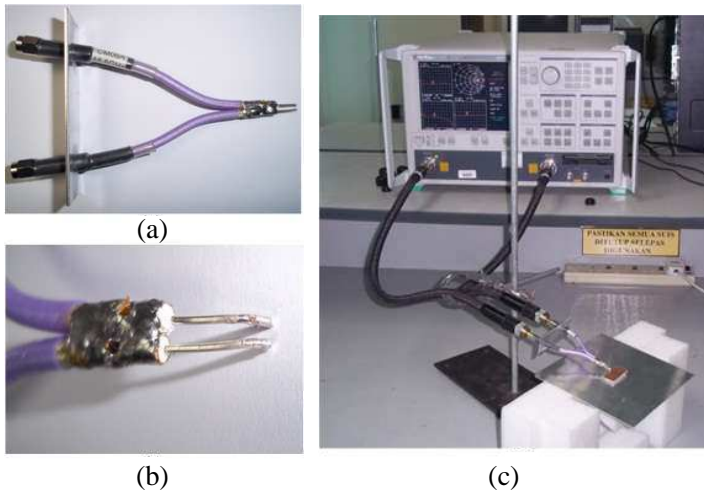


Figure 6. (a) Differential probe, (b) open-ended side of semirigid cables, and (c) measurement setup.

verify the tag antenna impedance. The probe is constructed by using two semirigid coaxial cables with a length of 120 mm and an outer conductor diameter of 3 mm as shown in Figure 6(a). One end of the two semirigid coaxial cables is soldered together on their outer conductors to form the common virtual ground (Figure 6(b)), while the inner conductors are open-ended and partially extended to be soldered to the antenna under test at the chip position. The other end of the probe is with two subminiature version A (SMA) connectors and connected to a Vector Network Analyzer, (VNA model: Anritsu 37347D) through the test cables. The measurement setup was performed in an ordinary room environment as shown in Figure 6(c).

Figure 7 shows the simulated and measured results for the impedance of the designed tag antenna. The measured results were obtained after deembedding the influence of the semirigid cables from the two-port S -parameters (S_{11} , S_{12} , S_{21} , and S_{22}). From Figure 7, we observed that there is little difference between the simulated and measured resistance curves at the operating frequency. However, the simulated and measured reactance curves are in a reasonably good agreement. They are intersecting with each other and with the design target curve at the operating frequency. The variation between these results may be originating from the non-ideal nature of the measurement probe; small mismatch between the feeding lines and SMA connectors, as well as defects of the Printed Circuit Board (PCB) fabrication process. Figure 7 also shows that the simulated and measured impedances are $(9 + j105) \Omega$ and $(13 + j104) \Omega$, respectively at the design frequency of 915 MHz.

Power Reflection Coefficient (PRC) Γ analysis used by [28] is adopted here. The tag design is required to provide impedance matching between two components, chip and antenna. The measured

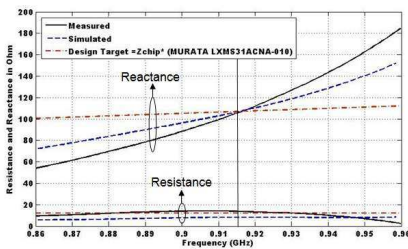


Figure 7. Impedance simulation and measurement results of the proposed antenna.

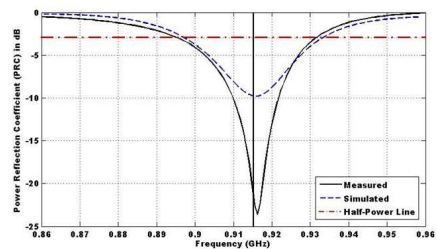


Figure 8. Simulated and measured PRC of the proposed tag antenna.

and simulated PRC curves of the implemented antenna with half-power bandwidth line are shown in Figure 8. The curves are based on the assumption that the real part of the chip impedance is not changing with frequency. The half-power bandwidth of the antenna is determined using the criterion $\Gamma < -3$ dB. The simulated half-power bandwidth is found to be 6.77% (896–934 MHz) at 915 MHz center frequency, while the measured value is 6.76% (894–932 MHz) at 917 MHz center frequency.

The maximum theoretical read range of the proposed RFID tag antenna can be calculated using Friis free-space formula [29]:

$$r_{\max} = \frac{\lambda}{4\pi} \sqrt{\frac{P_t G_t G_r}{P_{th}}} \quad (3)$$

where P_t is the power transmitted by the reader, G_t is the gain of the reader antenna, G_r is the gain of the receiving tag antenna, λ is the wavelength, and P_{th} is the minimum threshold power necessary to power up the chip. The product $P_t G_t$ is the Equivalent Isotropic Radiated Power (EIRP). The maximum theoretical read range calculated using (3) is 0.93 m. The read range is also measured using the ATid (AT-870) handheld reader. The reader's output power is set to 4.0 W EIRP. The tag was mounted on a square metal sheet of 0.5λ side length and 0.006λ thickness, while the operating frequency of the reader sweeps from 900 MHz to 930 MHz. The maximum measured read range was found to be 0.82 m. The deviation of the measured read range from the calculated one is due to the fact that the measurement was conducted in an ordinary room environment. The gain of the designed tag antenna is a trade off with its miniaturized structure. The antenna features a lowered read range because of the high minimum threshold power required to turn on the MURATA chip (160 μ W). The read range can be improved, even tripled, depending on the chip that is used. According to (3), using the Alien Higgs-3 chip [30] with minimum threshold power of -18 dBm (16 μ W) would give a maximum theoretical read range of 2.92 m.

Table 2. Variation of maximum read range for different values of metal sheet size.

Metal Sheet Side Length in cm	r_{\max} in m	
	Calculated	Measured
16	0.93	0.82
32	0.82	0.72
48	0.77	0.68

Figure 9 shows the simulation results of the antenna radiation pattern for different values of the metal sheet side length. It is clear from the figure that increasing the metal sheet size at the tag's background plane slightly decreases its gain and hence the read range. Table 2 summarizes the calculated and measured read range for different values of metal sheet size.

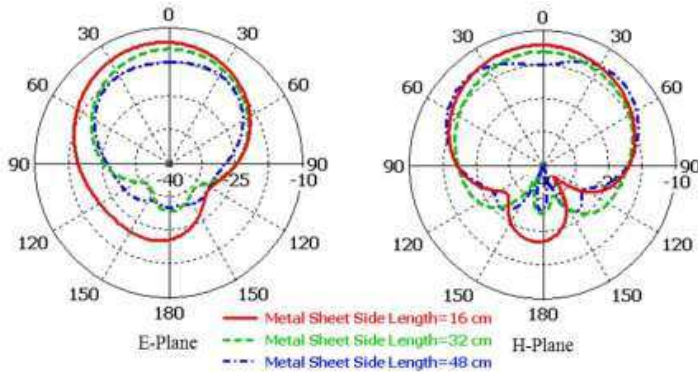


Figure 9. Simulation results of antenna radiation patterns with different values of metal sheet side length.

4. CONCLUSION

This paper presents a miniaturized RFID tag antenna, in which its configuration is optimized specifically to be mountable on metallic objects. The compact design is achieved by inserting a CSRR layer into the antenna structure, which lowers its resonant frequency by increasing the capacitive reactance and allows high reactive impedance. The size of the proposed tag antenna is $36.7 \times 18.1 \times 3.165 \text{ mm}^3$, and it is etched on a FR4 material substrate with thickness of 1.53 mm. A very small and compact tag antenna is achieved with good agreement between measured and simulated results. The experiment attested that the maximum read range of the prototype is obtained when the tag is placed on a metallic object, which is about 0.82 m with 4.0 W EIRP radiation power of the RFID reader. The proposed RFID tag antenna offers attractive design for metallic objects identification such as gas cylinders and oil barrels tagging in petrol refineries.

ACKNOWLEDGMENT

The authors wish to thank the Universiti Putra Malaysia for providing us the research fund (RUGS Project No.: 05-01-09-0722RU) to conduct this work. The authors would also like to thank the SENSTECH SDN BHD (728289-X), Kuala Lumpur, Malaysia, and those others that have helped in the project directly or indirectly.

REFERENCES

1. Kwon, H. and B. Lee, "Compact slotted planar inverted-F RFID tag mountable on metallic objects," *Electron. Lett.*, Vol. 41, No. 24, 1308–1310, 2005.
2. Son, H. W. and G. Y. Choi, "Orthogonally proximity-coupled patch antenna for a passive RFID tag on metallic surfaces," *Microw. Opt. Technol. Lett.*, Vol. 49, No. 3, 715–717, 2007.
3. Kim, J. S., W. Choi, and G. Y. Choi, "UHF RFID tag antenna using two PIFAs embedded in metallic objects," *Electron. Lett.*, Vol. 44, No. 20, 1181–1182, 2008.
4. Chen, H.-D. and Y.-H. Tsao, "Low-profile PIFA array antennas for UHF band RFID tags mountable on metallic objects," *IEEE Transactions on Antennas and Propagation*, Vol. 58, No. 4, 1087–1092, 2010.
5. Kim, K. H., J. G. Song, D. H. Kim, H. S. Hu, and J. H. Park, "Forkshaped RFID tag antenna mountable on metallic surfaces," *Electron. Lett.*, Vol. 43, No. 25, 1400–1402, 2007.
6. Chen, S.-L., "A miniature RFID tag antenna design for metallic objects application," *IEEE Antennas and Wireless Propagation Letters*, Vol. 8, 1043–1045, 2009.
7. Chaimool, S. and P. Akkaraekthalin, "A compact dual-band printed dipole antenna based on fractal feature in ISM band," *Proc. International Symposium on Antennas and Propagation (ISAP 2008)*, 27–30, 2008.
8. Lee, Y.-C. and J.-S. Sun, "Dual-band dipole antenna for RFID tag applications," *Proceedings of the 38th European Microwave Conference*, 995–997, 2008.
9. Kimouche, H. and H. Zemmour, "A compact fractal dipole antenna for 915 MHz and 2.4 GHz RFID tag applications," *Progress In Electromagnetics Research Letters*, Vol. 26, 105–114, 2011.
10. Zainud-Deen, S. H., H. A. Malhat, and K. H. Awadalla,

- “Fractal antenna for passive UHF RFID applications,” *Progress In Electromagnetics Research B*, Vol. 16, 209–228, 2009.
11. Gianvittorio, J. P. and Y. Rahmat-Samii, “Fractal antennas: A novel antenna miniaturization technique, and applications,” *IEEE Antennas and Propagation Magazine*, Vol. 44, No. 1, 20–36, Feb. 2002.
 12. Best, S. R., “A comparison of the resonant properties of small space-filling fractal antennas,” *IEEE Antennas and Wireless Propagation Letters*, Vol. 2, 197–200, 2003.
 13. Loo, C.-H., K. Elmahgoub, F. Yang, A. Elsherbeni, D. Kajfez, A. Kishk, T. Isherbeni, L. Ukkonen, L. Sydnheimo, M. Kivikoski, S. Merilampi, and P. Ruuskanen, “Chip impedance matching for UHF RFID tag antenna design,” *Progress In Electromagnetics Research*, Vol. 81, 359–370, 2008.
 14. Stutzman, W. L. and G. A. Thiele, *Antenna Theory and Design*, John Wiley & Sons, 1998.
 15. Palmer, K. D. and M. W. Rooyen, “Simple broadband measurements of balanced loads using a network analyzer,” *IEEE Transactions on Instrumentation and Measurement*, Vol. 55, No. 1, 266–272, 2006.
 16. Kuo, S.-K., S.-L. Chen, and C.-T. Lin, “An accurate method for impedance measurement of RFID tag antenna,” *Progress In Electromagnetics Research*, Vol. 83, 93–106, 2008.
 17. Qing, X., C. K. Goh, and Z. N. Chen, “Impedance characterization of RFID tag antennas and application in tag co-design,” *IEEE Transactions on Microwave Theory and Techniques*, Vol. 57, No. 5, 1268–1274, 2009.
 18. Kim, D., T. W. Koo, J.-I. Ryu, J.-G. Yook, and J. C. Kim, “Accurate impedance measurement and implementation of a folded dipole antenna for RFID tags,” *Proc. International Symposium on Antennas and Propagation (ISAP 2009)*, 2009.
 19. Marques, R., F. Mesa, J. Martel, and F. Medina, “Comparative analysis of edge- and broadside-coupled split ring resonators for metamaterial design — Theory and experiment,” *IEEE Transactions on Antennas and Propagation*, Vol. 51, No. 10, 2572–2581, 2003.
 20. Marques, R., F. Medina, and R. Rafi-El-Idrissi, “Role of bianisotropy in negative permeability and left handed metamaterials,” *Phys. Rev. B*, Vol. 65, 144440(1)–144440(6), 2002.
 21. Gay-Balmaz, P. and O. J. F. Martina, “Electromagnetic

- resonances in individual and coupled split-ring resonators,” *Journal of Applied Physics*, Vol. 92, No. 5, 2929–2936, 2002.
22. Baena, J. D., J. Bonache, F. Martín, and R. M. Sillero, “Equivalent-circuit models for split-ring resonators and complementary split-ring resonators coupled to planar transmission lines,” *IEEE Transactions on Microwave Theory and Techniques*, Vol. 53, No. 4, 1451–1461, 2005.
 23. Pendry, J. B., A. J. Holden, D. J. Robbins, and W. J. Stewart, “Magnetism from conductors and enhanced nonlinear phenomena,” *IEEE Transactions on Microwave Theory and Techniques*, Vol. 47, 2075–2084, Nov. 1999.
 24. Smith, D. R., W. J. Padilla, D. C. Vier, S. C. Nemat-Nasser, and S. Schultz, “Composite medium with simultaneously negative permeability and permittivity,” *Physical Review Letters*, Vol. 84, No. 18, May 2000.
 25. Falcone, F., T. Lopetegui, M. A. G. Laso, J. D. Baena, J. Bonache, M. Beruete, R. Marqués, F. Martín, and M. Sorolla, “Babinet principle applied to metasurface and metamaterial design,” *Physical Review Letters*, Vol. 93, 197401(1)–197401(4), 2004.
 26. Murata MAGICSTRAP® Application Note, Online Available: <http://www.murata.co.jp/products/rfid/index.html>.
 27. Computer Simulation Technology (CST) Microwave Studio, Version 2010, 2010.
 28. Nikitin, P. V., K. V. S. Rao, S. F. Lam, V. Pillai, R. Martinez, and H. Heinrich, “Power reflection coefficient analysis for complex impedances in RFID tag design,” *IEEE Transactions on Microwave Theory and Techniques*, Vol. 53, No. 9, 2721–2725, 2005.
 29. Rao, K. V. S., P. V. Nikitin, and S. F. Lamn, “Antenna design for UHF RFID tags: A review and a practical application,” *IEEE Transactions on Antennas and Propagation*, Vol. 53, No. 12, 3870–3876, Dec. 2005.
 30. Alien Higgs-3, Online Available: <http://www.prosign.dk/en/rfid-products/alien-technology/>.